Supporting Information

Design of High-Performance Pd-based Alloy Nanocatalysts for Direct Synthesis of H_2O_2

HaoxiangXu[a], DaojianCheng[a*], Yi Gao[b,*]

[a]International Research Center for Soft Matter, Beijing Key Laboratory of Energy Environmental Catalysis, State Key Laboratory of Organic-Inorganic Composites, Beijing University of Chemical Technology, Beijing100029, China

E-mail: chengdj@mail.buct.edu.cn

[b]Division of Interfacial Water and Key Laboratory of Interfacial Physics and Technology, Shanghai Institute of Applied Physics, Chinese Academy of Sciences, Shanghai 201800, China

E-mail: gaoyi@sinap.ac.cn

Supplementary Text

Section 1. Model Clusters

In this work, these Pd-based clusters with the lowest-energy atomic ordering are obtained at the empirical potential level[1-3] and then are subjected to DFT relaxation. The core is generally occupied by the doped metal according to the experimental results.[4-9] Taking the $Au_{25}Pd_{30}$ cluster with 13 of Au atoms fixed in the core as an example, the lowest-energy surface atomic ordering of such clusters is calculated at the empirical potential level[1-3] and the clusters are then subjected to DFT local relaxation. An EAM empirical potential[10-12] is used to model the metal-metal interactions, whose explicit form can be found elsewhere,[13, 11-12]as well as the parameters for Au–Pd which were taken from the literature.[14, 13]It is found that the lowest-energy surface atomic ordering of $Au_{25}Pd_{30}$ cluster turn out that the other 12 Au atoms occupy the vertex sites with 13 of Au atoms fixed in the core. It is noted that the lowest-energy atomic ordering and catalytic activity for direct synthesis of H_2O_2 of $Au_{25}Pd_{30}$ cluster without 13 of Au atoms fixed in the core were also calculated. Unfortunately, its activity and selectivity towards H_2O_2 is very low, which is also far away from the experimental results.[15] Detailed test process for this issue can be found in Section 8. Therefore, the resulting configurations of $Au_{25}Pd_{30}$with 13 of Au atoms fixed in the core are used to study adsorption and reaction properties, as shown in Figure 1. Accordingly, $Pt_{25}Pd_{30}$ and $Sn_{25}Pd_{30}$ has the same chemical ordering as $Au_{25}Pd_{30}$, which exclude the influence of chemical ordering in order to explore intrinsic effect of doped elements and compare with the available experiments. For the $Pt_2Au_{23}Pd_{30}$ cluster, compared with $Au_{25}Pd_{30}$, one Pt atom replaces Au atom in the center and the other Pt atom substitutes Au atom in the subsurface shell, which is in good agreement with the experimental characterization.[15]

Section 2: Determination of Adsorption Free Energies of Reaction Intermediates

We start by conducting a preliminary investigation on the adsorption of H_2, O_2, OOH, O, H, OH, H_2O and H_2O_2 on these clusters and identify the most preferable sites. Adsorption free energies of various reactants, intermediates, product species are

relative to the free energy of stoichiometrically appropriate amounts of $H_2O(g)$ and $H_2(g)$ (see below for details). The entropy and zero-point energy (ZPE) corrections in determining the adsorption free energy are summarized in the Table S2. Adsorption free energy values are given in Table S3.

$$\Delta G_{H2}^{*}=\Delta E_{H2}^{*}+\Delta ZPE-T\times\Delta S$$

$$\Delta G_{O2}^{*}=E_{O2}^{*}+2\times E_{H2}-2\times E_{H2O}-E^{*}+\Delta ZPE-T\times\Delta S$$

$$\Delta G_{O}^{*}=E_{O}^{*}+E_{H2}-E_{H2O}-E^{*}+\Delta ZPE-T\times\Delta S$$

$$\Delta G_{H}^{*}=E_{H}^{*}-0.5\times E_{H2}-E^{*}+\Delta ZPE-T\times\Delta S$$

$$\Delta G_{OH}^{*}=E_{OH}^{*}+0.5\times E_{H2}-E_{H2O}+\Delta ZPE-T\times\Delta S$$

$$\Delta G_{OOH}^{*}=E_{OOH}^{*}+1.5\times E_{H2}-2\times E_{H2O}+\Delta ZPE-T\times\Delta S$$

$$\Delta G_{H2O}^{*}=\Delta E_{H2O}^{*}+\Delta ZPE-T\times\Delta S$$

$$\Delta G_{H2O2}^{*}=E_{H2O2}^{*}+E_{H2}-2\times E_{H2O}-E^{*}+\Delta ZPE-T\times\Delta S$$

The asterisk (*) indicates an adsorbed species.

Some assumptions involved in these free energy relations are listed in the following:

• Entropies or ZPEs of Empty sites on the clusters can be neglected

•ZPEs were averaged over the values calculated for species on all six clusters

•Entropies of gas species taken from thermodynamic tables at 298K

•The entropies of intermediates adsorbed on clusters are negligible

Section 3: Adsorption Free Energy Scaling Relationships for Reaction Intermediates

As is generally accepted, the adsorption energy correlates with the binding energy of the atomic species when the adsorbates bind to the metal surface.[16-19] So the well-known scaling correlations that relate the adsorption free energy of cluster-bound adsorbates to appropriate descriptors are determined, such as

$$\Delta G_{OH}^{*}=\alpha*\Delta G_{O}^{*}+\beta$$

Similar correlations can be identified for all other oxygen-containing species and hydrogen-containing species based on the G_O* and G_H* descriptors, respectively. The determined scaling relations are plotted in Figure S1

Section 4: Reaction Barriers (G_a) and Reaction Free Energies (ΔG_r) in the Sabatier Analysis

We can then define thermodynamic reaction free energies of elementary steps by adsorption free energy. For example:

$$\Delta G_r(O^*+H^* \rightarrow OH^*)=\Delta G_{OH}{}^* - \Delta G_O{}^* - \Delta G_H{}^*$$

For hydrogenation steps, reaction free energies are regarded as approximate values of reaction barriers, since the neglect of over-barriers for highly endergonic hydrogenation steps has been proved as a very good approximation by many studies,[20-24] which is also verified from the comparison between ΔG_r and G_a in Table S4. This approximation may result in a slight overestimation of activity for a given hydrogenation elementary step, but can still qualitatively represent the right relative energetic ordering of the various hydrogenation steps. Therefore, the values of G_a for main reaction in Table S8 and Table S9 are substituted by ΔG_r

Additionally, activation barrier (G_a) of elementary dissociation via O-O/H-H bond breaking scales nearly linearly with the reaction free energy (ΔG_r), resulting in the BEP relation as shown in Figures S2. This is a very general trend and has been observed for a wide variety of other bond breaking reactions, such as C-C, N-N, C-O, N-O, and C-N.[25-26] Once these scaling relation analyses are in place, the G_a of catalysts for each elementary step in reaction network at each value of ΔG_O* and ΔG_H* can be rapidly evaluated, and the corresponding Sabatier activity can be established. It is noted that negative barriers in the rate-limiting step is not allowed near the very peak of the volcano, which produces a small region of essentially zero barrier near the top of the volcano. Nevertheless, coverage effects, together with small hydrogenation over barriers would modestly decrease the rate near the top of the volcano in a full microkinetic analysis.[27]

Section 5: Reaction Barrier Inequality Constraints

The Sabatier activity analysis alone is not sufficient to determine selectivity between elementary steps in main and side reaction pathways. From Figure 2, reactions involving O-O bond cleavage that will divert the catalyst away from the

direct hydrogen peroxide synthesis pathway. For example, it can be seen that, even if OOH formation is favored, subsequent dissociation to O* + OH*, which ultimately leads to water formation, may occur in the following reaction. In order to incorporate selectivity considerations into Sabatier activity analysis, a series of reaction barrier inequalities are identified. In order to be fully selective toward H_2O_2 for the system, all inequality constraints must be satisfied. Therefore, the selective hydrogen peroxide region of the Sabatier volcano toward H_2O_2 is the minimally intersecting region of the following reaction barrier inequalities:

$$G_{aO2*+H*\rightarrow OOH*} < G_{aO2* \rightarrow 2O*} \quad (1)$$

$$G_{aOOH*+H*\rightarrow H2O2*} < G_{aOOH*\rightarrow OH*+O*} \quad (2)$$

$$G_{aH2O2*\rightarrow H2O2\ (l)+*} < G_{aH2O2*\rightarrow 2OH*} \quad (3)$$

$$G_{aH2O2*\rightarrow H2O2\ (l)+*} < G_{aH2O2*\rightarrow H2O*\ +O*} \quad (4)$$

The selectivity criteria can be thought of qualitatively in the following manner. Inequality constraint 1 represents the competition between O_2 dissociation and hydrogenation that is relevant early in the reaction network. Inequality constraint 2 represents the tendency of OOH* hydrogenation to H_2O_2* as compared to its tendency to dissociate to OH*+O*. Inequality constraint 3 represents the competition between desorption of H_2O_2* into the solution phase and dissociation into 2OH*. Inequality constraint 4 describes the competition between H_2O_2* desorption and decomposition into O* +H_2O*. Since H_2 dissociation is an elementary step in all possible reaction pathways, this step is not involved in the selectivity criteria.

Section 6: DOS analysis of adsorbed O_2 on Pd_{55}, $Au_{25}Pd_{30}$, $Pt_{25}Pd_{30}$, $Sn_{25}Pd_{30}$ and $Pt_2Au_{23}Pd_{30}$

As is well-known, 5σ and 1π represent bonding orbit of O-O bond and region filled with red in Figure S5 is Lowest Unoccupied Molecular Orbit (LUMO). For elementary dissociation steps via O-O breaking, when 5σ orbit shift to Fermi level,

the O-O bond would become unstable with tendency to break. For elementary hydrogenation steps, a shift of 1π orbit to Fermi level can weaken O-O bond partly and a large region of LUMO is benefit to receive electron donation, which promote the formation of O-H bond. Compared with Pd_{55} in Figure 5a, $Pt_{25}Pd_{30}$ has less θ(Pd in shell) and reduce electron back-donation from Pd into 2π* orbits of the O−O bond, which makes 5σ orbit shift away from Fermi level and results in larger area of LUMO, as shown in Figure S5. Therefore, fewer θ(Pd in shell) in $Pt_{25}Pd_{30}$ than Pd_{55} may improve the activity for hydrogenation steps toward H_2O_2 and suppress the parallel H_2O_2 hydrogenation/decomposition pathways involving O−O bond cleavage. The similar conclusion can be drawn as comparing $Pt_{25}Pd_{30}$ and $Pt_2Au_{23}Pd_{30}$. Moreover, $Au_{25}Pd_{30}$ is of excessive fewer θ(Pd in shell) than $Pt_{25}Pd_{30}$, and the weakly adsorbed O_2 is hard to dissociate or be hydrogenated due to the too stable O-O bond (1π orbit is far away from Fermi level in spite of large region of LUMO in Figure S5.). Compared with $Pt_2Au_{23}Pd_{30}$, $Au_{25}Pd_{30}$ cluster with fewer θ(Pd in shell) would receive electron donation from adsorbed O_2 and weaken O-O bond slightly(5σ orbit shift to Fermi level a bit.), for which the ability to hinder side reaction in $Au_{25}Pd_{30}$ is in inferior to $Pt_2Au_{23}Pd_{30}$.

Section 7: Sabatier analysis for predicted Pd-based catalysts

As shown in Sabatier activity volcano of Figure S8a, $W_{25}Pd_{30}$ and $Pb_{25}Pd_{30}$ lie on the region with higher activity and selectivity than $Au_{25}Pd_{30}$, while other Pd-based binary nanocatalysts fail to be eligible catalyst due to the unsatisfactory activity and selectivity. Likewise, the promising new Pd-based ternary nanocatalysts predicted above, are $Mo_2Au_{23}Pd_{30}$, $Ru_2Au_{23}Pd_{30}$, $Os_2Au_{23}Pd_{30}$, $Ir_2Au_{23}Pd_{30}$, $Rh_2Au_{23}Pd_{30}$, $Pb_2Au_{23}Pd_{30}$ and $W_2Au_{23}Pd_{30}$, which are closer to the top of Sabatier activity volcano than $Pt_2Au_{23}Pd_{30}$ and $Ag_2Au_{23}Pd_{30}$, as shown in Figure S8b.

Section 8: Detailed test process for $Au_{25}Pd_{30}$ cluster with the lowest-energy atomic ordering

The lowest-energy atomic ordering of whole $Au_{25}Pd_{30}$ cluster (Figure S9) is also calculated at the empirical potential level. However, its activity for main/side reaction

by DFT calculation (Table S11) don't match the high selectivity of experiment result, because it is found to be high molar surface Au/Pd ratio which is not in line with XPS-analysis.[15]

Reference

(1) Cheng, D.; Huang, S.; Wang, W. *Phys. Rev. B* **2006**, *74*, 064117.

(2) Cheng, D.; Liu, X.; Cao, D.; Wang, W.; Huang, S. *Nanotechnology* **2007**, *18*, 162-193.

(3) Cheng, D.; Wang, W. *Nanoscale* **2012**, *4*, 2408-2415.

(4) Edwards, J. K.; Carley, A. F.; Herzing, A. A.; Kiely, C. J.; Hutchings, G. J. *Faraday Discuss.* **2008**, *138*, 225-239.

(5) Edwards, J. K.; Ntainjua N, E.; Carley, A. F.; Herzing, A. A.; Kiely, C. J.; Hutchings, G. J. *Angew. Chem., Int.Ed.* **2009**, *48*, 8512-8515.

(6) Herzing, A. A.; Watanabe, M.; Edwards, J. K.; Conte, M.; Tang, Z. R.; Hutchings, G. J.; Kiely, C. J. *Faraday Discuss.* **2008**, *138*, 337-351.

(7) Pritchard, J. C.; He, Q.; Ntainjua, E. N.; Piccinini, M.; Edwards, J. K.; Herzing, A. A.; Carley, A. F.; Moulijn, J. A.; Kiely, C. J.; Hutchings, G. J. *Green Chem.* **2010**, *12*, 915-921.

(8) Pritchard, J. C.; Kesavan, L.; Piccinini, M.; He, Q.; Tiruvalam, R.; Dimitratos, N.; Lopez-Sanchez, J. A.; Carley, A. F.; Edwards, J. K.; Kiely, C. J.; Hutchings, G. J. *Langmuir* **2010**, *26*, 16568-16577.

(9) Tiruvalam, R. C.; Pritchard, J. C.; Dimitratos, N.; Lopez-Sanchez, J. A.; Edwards, J. K.; Carley, A. F.; Hutchings, G. J.; Kiely, C. J. *Faraday Discuss.* **2011**, 63-86.

(10) Cheng, D.; Atanasov, I. S.; Hou, M. *Eur. Phys. J. D* **2011**, *64*, 37-44.

(11) Johnson, R. A. *Phys. Rev. B* **1989**, *39*, 12554-12559.

(12) Johnson, R. A. *Phys. Rev. B* **1990**, *41*, 9717-9720.

(13) Atanasov, I. S.; Hou, M. *Eur. Phys. J. D* **2009**, *52*, 51-54.

(14) Atanasov, I.; Hou, M. *Surf. Sci.* **2009**, *603*, 2639-2651.

(15) Edwards, J. K.; Pritchard, J. C.; Lu, L.; Piccinini, M.; Shaw, G.; Carley, A. F.; Morgan, D. J.; Kiely, C. J.; Hutchings, G. J. *Angew. Chem., Int.Ed.* **2014**, *53*, 2381-2384.

(16) Abild-Pedersen, F.; Greeley, J.; Studt, F.; Rossmeisl, J.; Munter, T. R.; Moses, P. G.; Skúlason, E.; Bligaard, T.; Nørskov, J. K. *Phys. Rev. Lett.* **2007**, *99*, 016105.

(17) Calle-Vallejo, F.; Loffreda, D.; Koper, M. T. M.; Sautet, P. *Nat. Chem.* **2015**, *7*, 403-410.

(18) Calle-Vallejo, F.; Martínez, J. I.; García-Lastra, J. M.; Rossmeisl, J.; Koper, M. T. M. *Phys. Rev. Lett.* **2012**, *108*, 1-5.

(19) Koper, M. T. M. *J. Electroanal. Chem.* **2011**, *660*, 254-260.

(20) Grabow, L. C.; Gokhale, A. A.; Evans, S. T.; Dumesic, J. A.; Mavrikakis, M. *J. Phys. Chem. C* **2008**, *112*, 4608-4617.

(21) Hyman, M. P.; Medlin, J. W. *J. Phys. Chem. B* **2006**, *110*, 15338-15344.

(22) Kandoi, S.; Gokhale, A. A.; Grabow, L. C.; Dumesic, J. A.; Mavrikakis, M. *Catal. Lett.* **2004**, *93*, 93-100.

(23) Nørskov, J. K.; Rossmeisl, J.; Logadottir, A.; Lindqvist, L.; Kitchin, J. R.; Bligaard, T.; Jónsson, H. *J. Phys. Chem. B* **2004**, *108*, 17886-17892.

(24) Tripković, V.; Skúlason, E.; Siahrostami, S.; Nørskov, J. K.; Rossmeisl, J. *Electrochim. Acta* **2010**, *55*, 7975-7981.

(25) Grabow, L. C.; Hvolbæk, B.; Falsig, H.; Nørskov, J. K. *Top. Catal.* **2012**, *55*, 336-344.

(26) Wang, S.; Temel, B.; Shen, J.; Jones, G.; Grabow, L. C.; Studt, F.; Bligaard, T.; Abild-Pedersen, F.; Christensen, C. H.; Nørskov, J. K. *Catal. Lett.* **2011**, *141*, 370-373.

(27) Nørskov, J. K.; Bligaard, T.; Hvolbaek, B.; Abild-Pedersen, F.; Chorkendorff, I.; Christensen, C. H. *Chem. Soc. Rev.* **2008**, *39*, 2163-2171.

(28) Freakley, S. J.; He, Q.; Harrhy, J. H.; Lu, L.; Crole, D. A.; Morgan, D. J.; Ntainjua, E. N.; Edwards, J. K.; Carley, A. F.; Borisevich, A. Y.; Kiely, C. J.; Hutchings, G. J. *Science* **2016**, *351*, 965-968.

Tables and Figures

Table S1: Mean particle size, alloy compositions, atom arrangement and preparation method from cited experimental work

Model	Size/nm	Compositions	Arrangement	Method	Ref
Au_{55}	1.2	100%Au		impregnation	[15]
Pt_{55}	1.2	100%Pt		impregnation	[15]
Pd_{55}	1.2	100%Pd		impregnation	[15]
$Au_{25}Pd_{30}$	1.2	50%Au-50%Pd	Au-core/Pd-shell	impregnation	[15]
$Sn_{25}Pd_{30}$	5	40%Sn-60%Pd	Sn-core/Pd-shell	impregnation	[28]
$Pt_{25}Pd_{30}$	1.2	50%Pt-50%Pd	Pt-core/Pd-shell	impregnation	[15]
$Pt_2Au_{23}Pd_{30}$	1.5	4%Pt-46%Au-50%Pd	Au,Pt-core/Pd-shell	impregnation	[15]

Table S2: Values used for the entropy and zero-point energy corrections in determining the free energy of reactants, products, and intermediate species adsorbed on clusters. For the surface bound species, the ZPE values are averaged over selected clusters.

Species	T×S (kJ/mol) (298K)	ZPE (kJ/mol)
H^*	0	16.39
O^*	0	6.75
H_2^*	0	23.15
O_2^*	0	8.68
OH^*	0	31.82
OOH^*	0	41.47
H_2O^*	0	48.22
$H_2O_2^*$	0	64.61
H_2(g)	39.54	26.04
H_2O(g)	55.93	54.97

Table S3: DFT-Computed Adsorption Free Energies (kJ/mol) of the Various Adsorbates on the Clusters[a]

	Adsorbate species free energy							
Composition	O	H	O_2	H_2	OH	OOH	H_2O_2	H_2O
Au_{55}	232.42	9.64	531.38	35.68	145.62	492.80	441.69	33.75
Pt_{55}	142.73	-45.33	353.93	-33.75	60.76	372.25	351.04	17.36
Pd_{55}	119.58	-28.93	340.43	-9.64	47.25	359.72	345.25	14.47
$Au_{25}Pd_{30}$	151.41	-47.25	389.61	-37.61	74.26	394.43	363.57	23.15
$Pt_{25}Pd_{30}$	107.05	-29.90	305.71	-14.47	40.50	319.21	327.89	9.64
$Sn_{25}Pd_{30}$	135.98	-40.50	354.89	-27.97	63.65	367.43	351.04	16.39
$Pt_2Au_{23}Pd_{30}$	179.38	-37.61	417.58	-19.29	113.80	404.08	372.25	27.97

[a]Units of free energy are given are in eV relative to the free energy of stoichiometrically appropriate amounts of H_2O(g) and H_2(g). Additional information on entropies and zero point energies is given in the Supporting Information.

Table S4: Reaction barrier (G_a,kJ/mol) and reaction free energy (ΔG_r,kJ/mol) of elementary reactions on Au_{55}, Pt_{55}, Pd_{55}, $Au_{25}Pd_{30}$, $Pt_{25}Pd_{30}$, $Sn_{25}Pd_{30}$ and $Pt_2Au_{23}Pd_{30}$ clusters. The asterisk (*) indicates an adsorbed species.

Reaction	Au_{55}		Pt_{55}		Pd_{55}		$Au_{25}Pd_{30}$		$Pt_{25}Pd_{30}$		$Sn_{25}Pd_{30}$		$Pt_2Au_{23}Pd_{30}$	
	G_a	ΔG_r	G_a	ΔG_r	G_a	ΔG_r	G_a	ΔG_r	G_a	ΔG_r	G_a	ΔG_r	G_a	ΔG_r
Dissociation														
1) $H_2^* \rightarrow 2H^*$	80.04	-16.39	0.00	-56.90	0.00	-48.22	0.00	-56.90	0.00	-45.33	0.00	-53.04	0.00	-55.93
2) $O_2^* \rightarrow 2O^*$	67.51	-66.54	65.58	-69.44	14.47	-101.26	48.22	-86.79	34.72	-90.65	49.18	-82.94	91.62	-58.83
3) $OOH^* \rightarrow OH^* + O^*$	77.15	-114.76	32.79	-169.73	7.72	-191.91	39.54	-168.77	26.04	-170.70	35.68	-167.80	84.87	-110.90
4) $H_2O_2^* \rightarrow 2OH^*$	74.26	-151.41	28.93	-230.49	7.72	-249.78	37.61	-215.06	12.54	-245.92	28.93	-223.74	81.97	-145.62
5) $H_2O_2^* \rightarrow H_2O^* + O^*$	75.22	-176.48	35.68	-191.91	0.96	-211.20	39.54	-189.02	4.82	-210.24	31.82	-198.66	87.76	-164.91
Hydrogenation														
6) $O_2^* + H^* \rightarrow OOH^*$	8.68	-48.22	73.29	63.65	53.04	48.22	58.83	51.11	44.36	42.43	60.76	53.04	27.97	24.11
7) $OOH^* + H^* \rightarrow H_2O_2^*$	4.82	-60.76	27.97	24.11	17.36	14.47	23.15	16.39	39.54	38.58	28.93	24.11	13.50	5.79
8) $O^* + H^* \rightarrow OH^*$	0.00	-96.44	2.89	-36.65	0.00	-43.40	0.00	-29.90	0.00	-36.65	1.93	-31.82	3.86	-27.97
9) $OH^* + H^* \rightarrow H_2O^* + *$	0.00	-121.51	9.64	1.93	1.93	-4.82	2.89	-3.86	5.79	-0.96	2.89	-6.75	0.00	-48.22
Desorption														
10) $H_2O^* \rightarrow H_2O + *$	—	-33.75	—	-17.36	—	-14.47	—	-23.15	—	-9.64	—	-16.39	—	-27.97
11) $H_2O_2^* \rightarrow H_2O_2 + *$	—	-441.69	—	-351.04	—	-345.25	—	-363.57	—	-327.89	—	-351.04	—	-372.25

Table S5: Reaction Pathway, Activation Energy (kJ/mol) of rate-limiting step (marked in red), Activity (As) (kJ/mol) of main reaction for selected model. Hydrogen peroxide productivity rate ($mol_{H2O2}kg_{cat}^{-1}h^{-1}$) measured in experiments for catalyst with corresponding composition.

Model	Reaction path	G_a	As	Composition	Rate
Monometal					
Au_{55}	1,6,7,11	80.04	-80.04	100%Au	1[15]
Pt_{55}	1,6,7,11	73.29	-73.29	100%Pt	8[15]
Pd_{55}	1,6,7,11	53.04	-53.04	100%Pd	97[15]
Bimetal					
$Au_{25}Pd_{30}$	1,6,7,11	58.83	-58.83	50%Au-50%Pd	68[15]
$Sn_{25}Pd_{30}$	1,6,7,11	60.76	-60.76	40%Sn-60%Pd	61[28]
$Pt_{25}Pd_{30}$	1,6,7,11	44.36	-44.36	50%Pt-50%Pd	138[15]
Trimetal					
$Pt_2Au_{23}Pd_{30}$	1,6,7,11	27.97	-27.97	4%Pt-46%Au-50%Pd	155[15]

Table S6: Reaction Pathway, Activation Energy (kJ/mol) of rate-limiting step (marked in red), Activity (As) (kJ/mol) of side reaction for selected model. Hydrogen peroxide hydrogenation/decomposition rate ($mol_{H2O2}kg_{cat}^{-1}h^{-1}$) measured in experiments for catalyst with corresponding composition.

Model	Reaction path	G_a	As	Composition	Rate
monometal					
Au_{55}	1,2,8,9,10	80.04	-80.04	100%Au	118[15]
	1,6,3,9,10	80.04			
	1,6,7,4,9,10	80.04			
	1,6,7,5,10	80.04			
Pt_{55}	1,2,8,9,10	65.58	-65.58	100%Pt	126[15]
	1,6,3,9,10	73.29			
	1,6,7,4,9,10	73.29			
	1,6,7,5,10	73.29			
Pd_{55}	1,2,8,9,10	14.47	-14.47	100%Pd	326[15]
	1,6,3,9,10	53.04			
	1,6,7,4,9,10	53.04			
	1,6,7,5,10	53.04			
Bimetal					
$Au_{25}Pd_{30}$	1,2,8,9,10	48.22	-48.22	50%Au-50%Pd	145[15]
	1,6,3,9,10	58.83			
	1,6,7,4,9,10	58.83			
	1,6,7,5,10	58.83			
$Pt_{25}Pd_{30}$	1,2,8,9,10	34.72	-34.72	50%Pt-50%Pd	182[15]
	1,6,3,9,10	44.36			
	1,6,7,4,9,10	44.36			
	1,6,7,5,10	44.36			
$Sn_{25}Pd_{30}$	1,2,8,9,10	28.93	-28.93	40%Sn-60%Pd	65[28]
	1,6,3,9,10	60.76			
	1,6,7,4,9,10	60.76			
	1,6,7,5,10	60.76			
Trimetal					
$Pt_2Au_{23}Pd_{30}$	1,2,8,9,10	91.62	-81.97	4%Pt-46%Au-50%Pd	94[15]
	1,6,3,9,10	84.87			
	1,6,7,4,9,10	81.97			
	1,6,7,5,10	87.76			

Table S7: Electronegativity (E_M) and corresponding descriptor α of doped elements

Dopant	E_M	α	Dopant	E_M	α	Dopant	E_M	α
Sc	1.36	0.62	Y	1.22	0.55	Hf	1.32	0.60
Ti	1.54	0.70	Zr	1.33	0.60	Ta	1.51	0.69
V	1.63	0.74	Nb	1.59	0.72	W	2.36	1.07
Cr	1.66	0.75	Mo	2.16	0.98	Re	1.93	0.88
Mn	1.55	0.70	Ru	2.2	1.00	Os	2.18	0.99
Fe	1.83	0.83	Rh	2.28	1.04	Ir	2.2	1.00
Co	1.88	0.85	Pd	2.2	1.00	Pt	2.28	1.04
Ni	1.92	0.87	Ag	1.93	0.88	Au	2.54	1.15
Cu	1.9	0.86	Cd	1.69	0.77	Hg	2	0.91
Zn	1.65	0.75	In	1.78	0.81	Tl	1.62	0.74
Ga	1.81	0.82	Sn	1.96	0.89	Pb	2.33	1.06
Ge	2.01	0.91	Sb	2.05	0.93	Bi	2.02	0.92

Table S8: Calculated free adsorption energy (kJ/mol) of O and H, Reaction Pathway, Predicted activation energy (kJ/mol) of rate-limiting step (marked in red), Predicted activity (kJ/mol) of main and side reaction for Pd-based binary alloys.

Model	ΔG_O^*	ΔG_H^*	Main reaction			Side reaction		
			Path	G_a	Activity	Path	G_a	Activity
$Ag_{25}Pd_{30}$	90.65	-39.54	1,6,7,11	71.36	-71.36	1,2,8,9,10	25.07	-25.07
						1,6,3,9,10	71.36	
						1,6,7,4,9,10	71.36	
						1,6,7,5,10	71.36	
$Rh_{25}Pd_{30}$	126.33	-27.97	1,6,7,11	42.43	-42.43	1,2,8,9,10	40.50	-40.50
						1,6,3,9,10	42.43	
						1,6,7,4,9,10	42.43	
						1,6,7,5,10	42.43	
$Os_{25}Pd_{30}$	105.12	-31.82	1,6,7,11	54.01	-54.01	1,2,8,9,10	32.79	-32.79
						1,6,3,9,10	54.01	
						1,6,7,4,9,10	54.01	
						1,6,7,5,10	54.01	
$W_{25}Pd_{30}$	188.05	-43.40	1,6,7,11	28.93	-28.93	1,2,8,9,10	66.54	-60.76
						1,6,3,9,10	60.76	
						1,6,7,4,9,10	60.76	
						1,6,7,5,10	62.68	
$Pb_{25}Pd_{30}$	186.13	-41.47	1,6,7,11	27.97	-27.97	1,2,8,9,10	65.58	-59.79
						1,6,3,9,10	59.79	
						1,6,7,4,9,10	59.79	
						1,6,7,5,10	61.72	

Table S9: Calculated free adsorption energy (kJ/mol) of O and H, Reaction Pathway, Predicted activation energy (kJ/mol) of rate-limiting step (marked in red), Predicted activity (kJ/mol) of main and side reaction for AuPd-based ternary alloys.

Model	ΔG_O^*	ΔG_H^*	Main reaction			Side reaction		
			Path	G_a	Activity	Path	G_a	Activity
$Ag_2Au_{23}Pd_{30}$	162.98	-49.18	1,6,7,11	47.25	-47.25	1,2,8,9,10	55.93	-45.33
						1,6,3,9,10	47.25	
						1,6,7,4,9,10	45.33	
						1,6,7,5,10	46.29	
$Rh_2Au_{23}Pd_{30}$	215.06	-45.33	1,6,7,11	18.32	-18.32	1,2,8,9,10	78.12	-76.19
						1,6,3,9,10	76.19	
						1,6,7,4,9,10	77.15	
						1,6,7,5,10	80.84	
$Os_2Au_{23}Pd_{30}$	211.20	-43.40	1,6,7,11	18.32	-18.32	1,2,8,9,10	76.19	-74.26
						1,6,3,9,10	74.26	
						1,6,7,4,9,10	75.22	
						1,6,7,5,10	77.15	
$W_2Au_{23}Pd_{30}$	182.27	-34.72	1,6,7,11	23.15	-23.15	1,2,8,9,10	63.65	-56.90
						1,6,3,9,10	57.86	
						1,6,7,4,9,10	56.90	
						1,6,7,5,10	58.83	
$Pb_2Au_{23}Pd_{30}$	184.20	-33.75	1,6,7,11	21.22	-21.22	1,2,8,9,10	64.61	-58.83
						1,6,3,9,10	58.83	
						1,6,7,4,9,10	58.83	
						1,6,7,5,10	59.79	
$Ru_2Au_{23}Pd_{30}$	209.27	-40.50	1,6,7,11	16.39	-16.39	1,2,8,9,10	75.22	-72.33
						1,6,3,9,10	72.33	
						1,6,7,4,9,10	73.29	
						1,6,7,5,10	76.19	
$Ir_2Au_{23}Pd_{30}$	200.59	-41.47	1,6,7,11	21.22	-21.22	1,2,8,9,10	71.36	-67.51
						1,6,3,9,10	67.51	
						1,6,7,4,9,10	68.47	
						1,6,7,5,10	70.40	
$Mo_2Au_{23}Pd_{30}$	180.34	-35.68	1,6,7,11	25.07	-25.07	1,2,8,9,10	63.65	-55.93
						1,6,3,9,10	56.90	
						1,6,7,4,9,10	55.93	
						1,6,7,5,10	57.86	

Table S10: Reaction Pathway, Calculated activation barriers (kJ/mol) of rate-limiting step (marked in red), Calculated activity (kJ/mol) of main and side reaction for predicted Pd-based alloys.

Model	Main reaction			Side reaction		
	Path	G_a	Activity	Path	G_a	Activity
$W_{25}Pd_{30}$	1,6,7,11	23.15	-23.15	1,2,8,9,10 1,6,3,9,10 1,6,7,4,9,10 1,6,7,5,10	66.54 55.93 58.83 56.90	-55.93
$Pb_{25}Pd_{30}$	1,6,7,11	37.61	-37.61	1,2,8,9,10 1,6,3,9,10 1,6,7,4,9,10 1,6,7,5,10	55.93 53.04 51.11 52.08	-51.11
$Ru_2Au_{23}Pd_{30}$	1,6,7,11	24.11	-24.11	1,2,8,9,10 1,6,3,9,10 1,6,7,4,9,10 1,6,7,5,10	65.58 62.68 58.83 60.76	-58.83
$Rh_2Au_{23}Pd_{30}$	1,6,7,11	13.50	-13.50	1,2,8,9,10 1,6,3,9,10 1,6,7,4,9,10 1,6,7,5,10	103.19 88.72 87.76 93.55	-87.76
$Os_2Au_{23}Pd_{30}$	1,6,7,11	22.18	-22.18	1,2,8,9,10 1,6,3,9,10 1,6,7,4,9,10 1,6,7,5,10	76.19 74.26 62.68 63.65	-62.68

Table S11: Reaction Pathway, Calculated activation barriers (kJ/mol) of rate-limiting step (marked in red), Calculated activity (kJ/mol) of main and side reaction for $Au_{25}Pd_{30}$ with lowest-energy atomic ordering.

Model	Main reaction			Side reaction		
	Path	G_a	Activity	Path	G_a	Activity
$Au_{25}Pd_{30}$(LEAO)	1,6,7,11	75.22	-75.22	1,2,8,9,10 1,6,3,9,10 1,6,7,4,9,10 1,6,7,5,10	36.65 75.22 75.22 75.22	-36.65

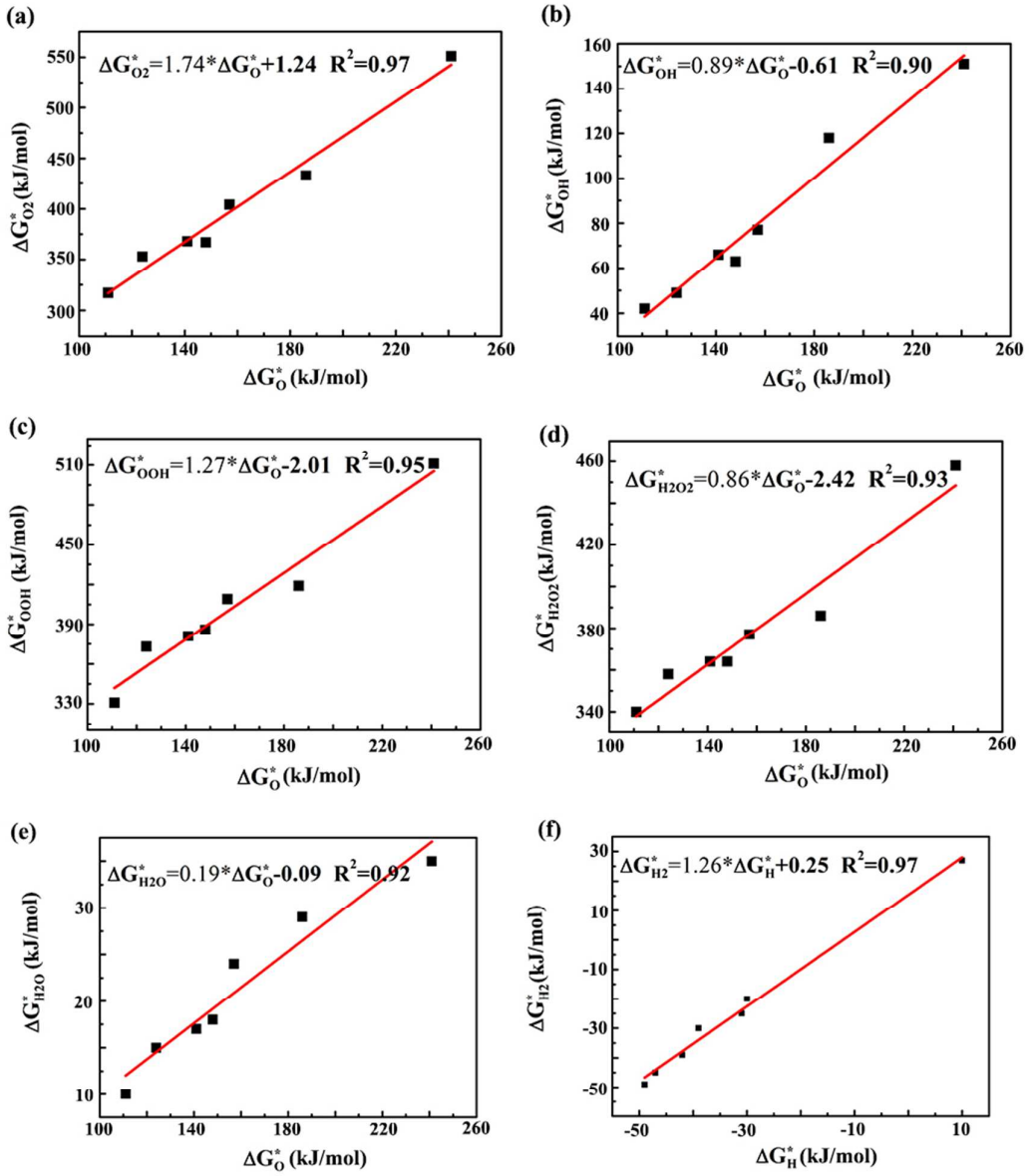

Figure S1: The determined scaling relations between the oxygen-containing species and ΔG_O^*, between the hydrogen-containing species and ΔG_H^*

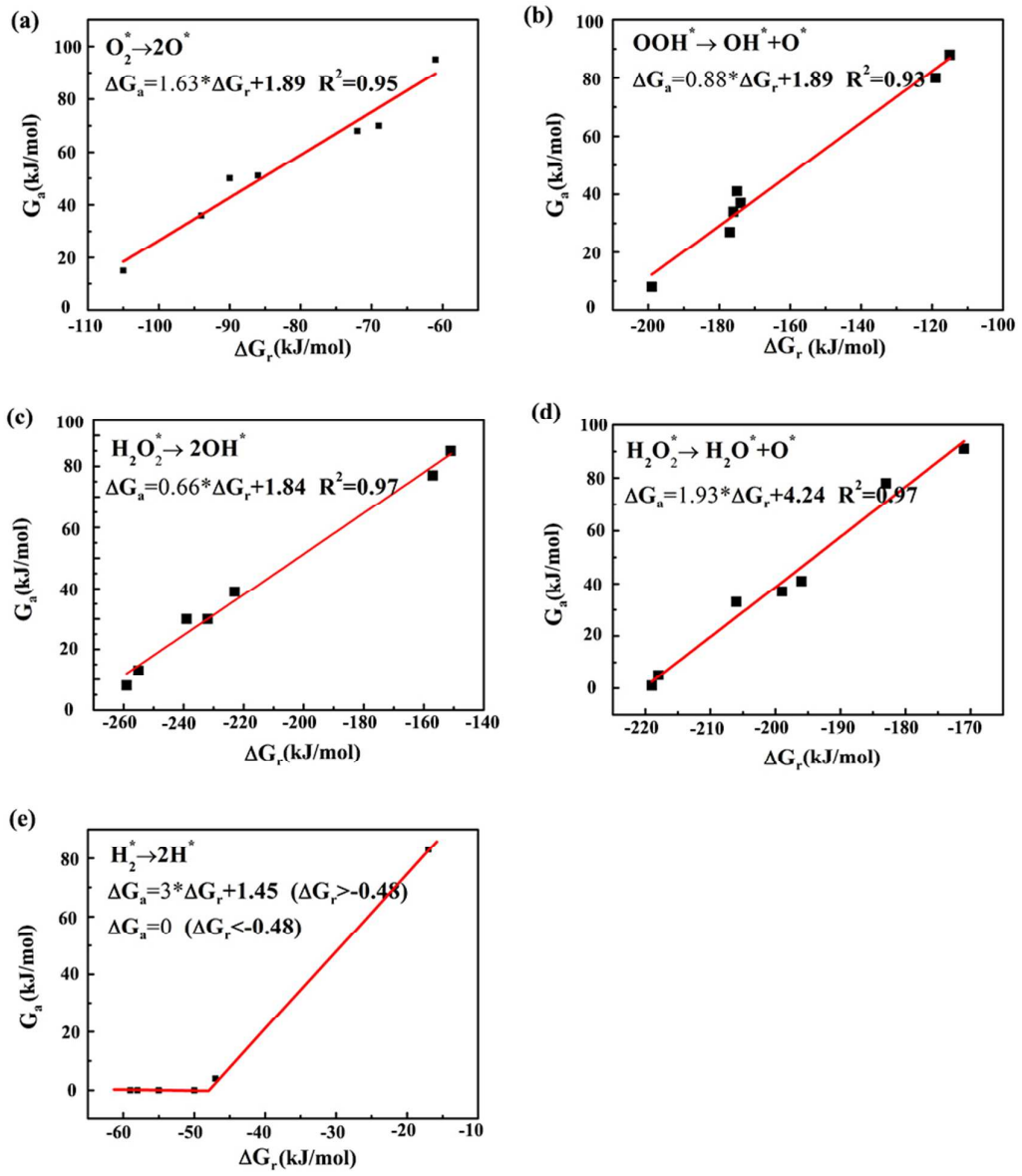

Figure S2: The determined BEP scaling relations between G_a and ΔG_r for the oxygen/hydrogen-containing dissociation process.

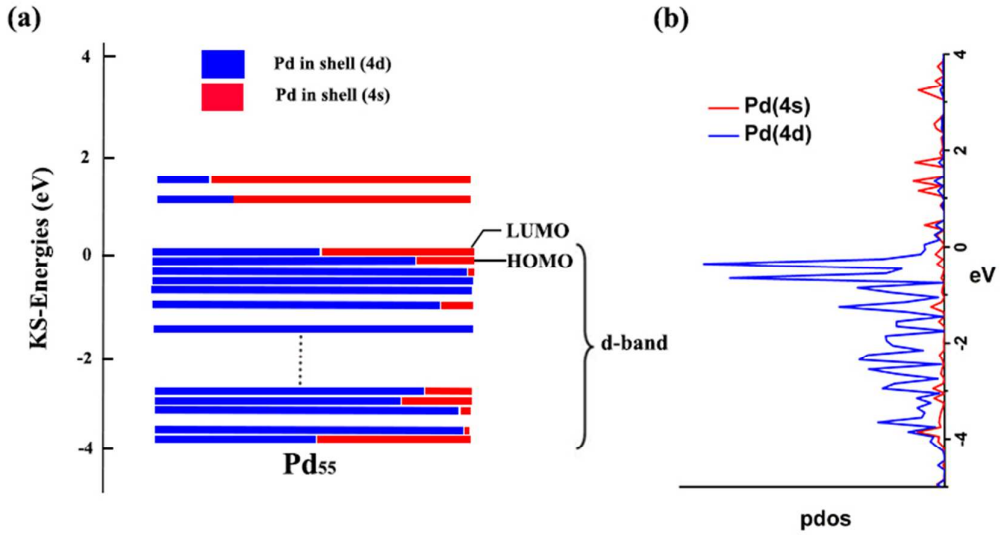

Figure S3: (a) Kohn–Sham orbital energy level diagram for Pd atoms in shell of Pd_{55}. Each KS orbital is drawn to indicate the relative contributions (line length with color labels) of the atomic orbitals of Pd (4s) in red, Pd (4d) in blue. The right column of the KS orbitals shows the HOMO and LUMO sets. (b) Projected density of states (pdos) for Pd atoms in shell of Pd_{55}.

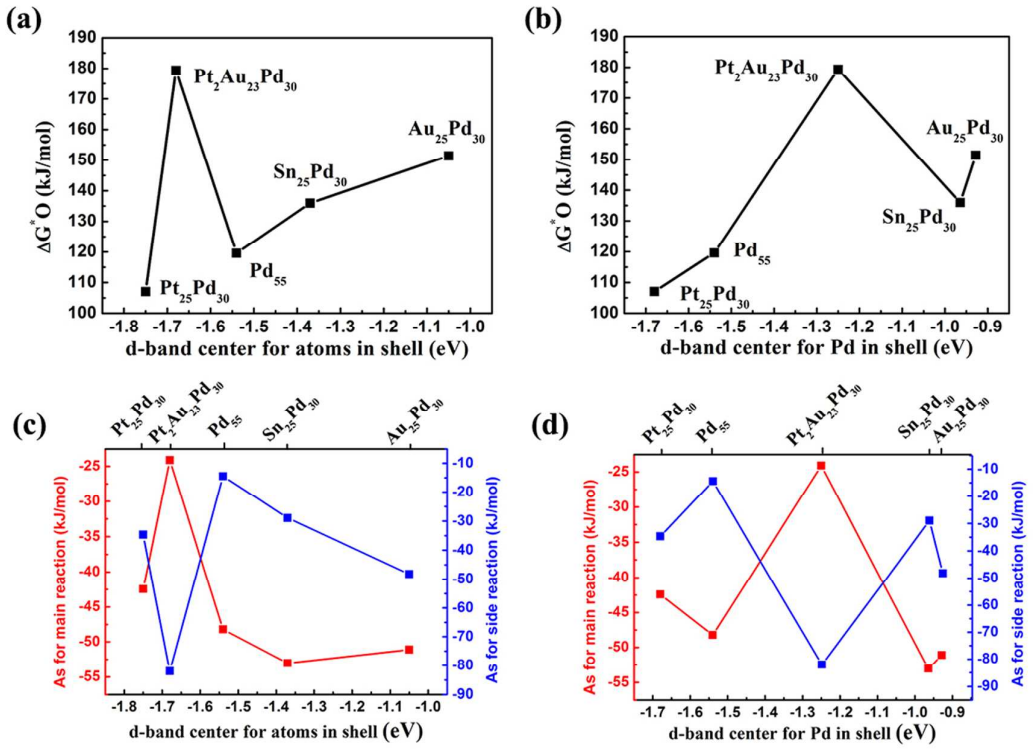

Figure S4: Adsorption free energy of O atom as a function of (a) d-band center for atoms in shell and (b) d-band center for Pd in shell of model systems. Main reaction activity and side reaction activity as a function of (c) d-band center for atoms in shell and (d) d-band center for Pd in shell of model systems.

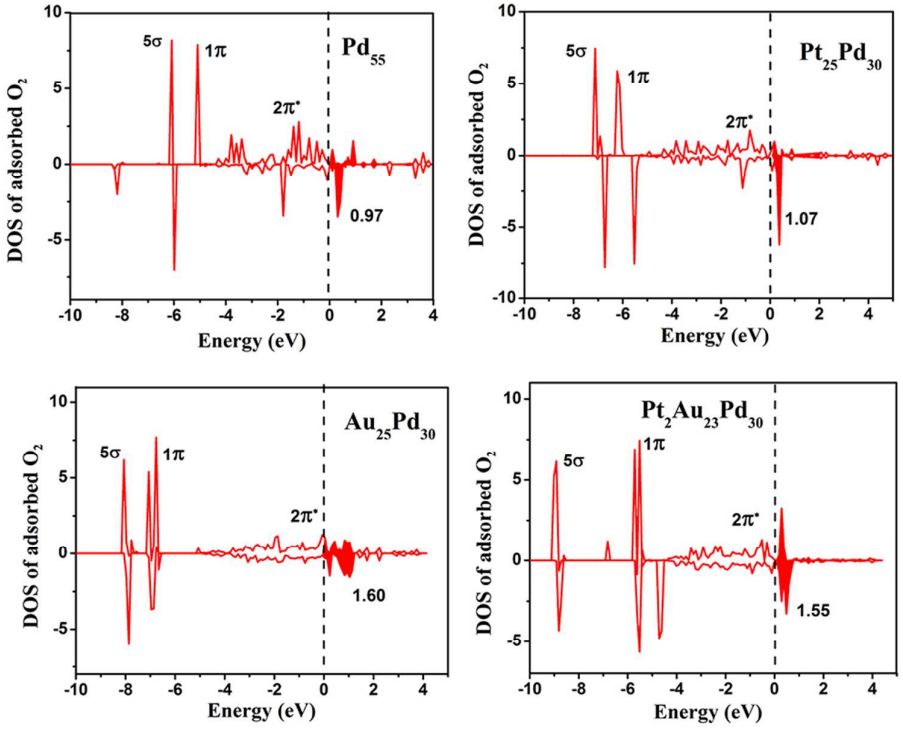

Figure S5: DOS of adsorded O_2 on Pd_{55}, $Au_{25}Pd_{30}$, $Pt_{25}Pd_{30}$ and $Pt_2Au_{23}Pd_{30}$ clusters. The dash lines represent Fermi level.

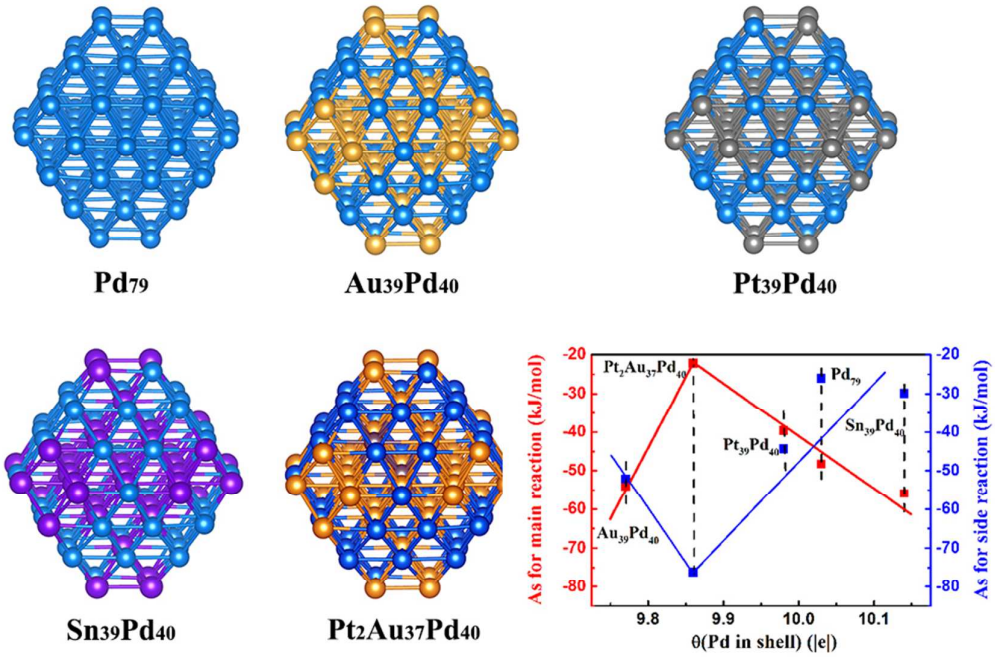

Figure S6. Schematic structures (yellow spheres, Au; blue spheres, Pd; gray spheres, Pt; purple spheres, Sn) of Pd_{79}, $Pt_{39}Pd_{40}$, $Au_{39}Pd_{40}$, $Sn_{39}Pd_{40}$ and $Pt_2Au_{37}Pd_{40}$ clusters. Calculated As for main reaction and side reaction as a function of average valance electron charge of Pd atoms in cluster shell.

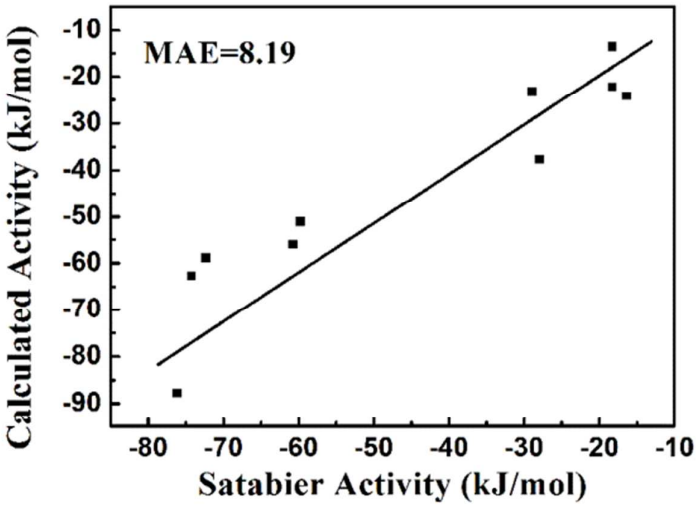

Figure S7: Calculated activity as a function of predicted Satabier activity for main/side reaction on different predicted Pd-based alloys nanocatalysts. Datas comes from Table S8~10.

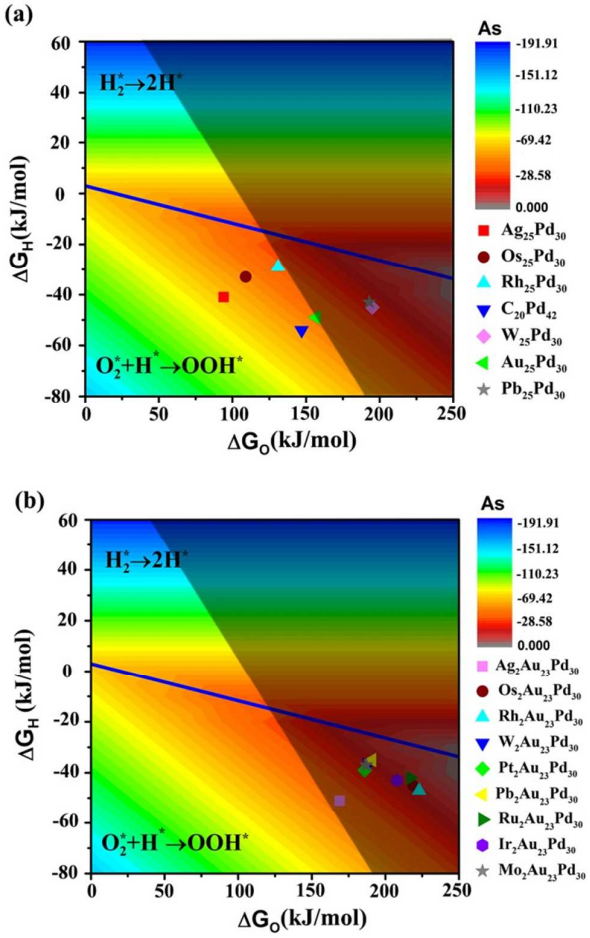

Figure S8: Activity volcano for direct oxygen reduction. ΔG_O*and ΔG_H* are the adsorption free energies of oxygen and hydrogen adsorption, respectively. The activity, in kJ/mol, is plotted as a function of both ΔG_O*and ΔG_H*. In the above regions, the predicted rate-controlling steps in each region of descriptor space are shown. The dash area is the selective hydrogen peroxide region of the Sabatier volcano toward H_2O_2, which satisfy all of the selectivity reaction barrier inequalities in the text. The values for different Pd-based alloys can be taken from their indicated positions.

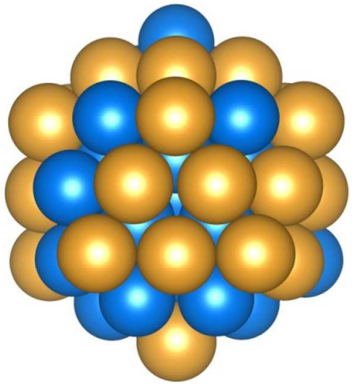

Figure S9: Schematic structures (yellow spheres, Au; blue spheres, Pd) of $Au_{25}Pd_{30}$ cluster with the lowest-energy atomic ordering.